International Journal of Engineering Trends and Technology
ISSN: 2231 – 5381 /doi:10.14445/22315381/IJETT-V69I9P230
Volume 69 Issue 9, 251-256, September, 2021
©2021 Seventh Sense Research Group®

Original Article

Study of Wall Climbing Robot Structure and Driving Torque Analysis

Yeon Taek OH

School of Mechanical Engineering, Tongmyung University, 428 Sinseon-ro, Nam-gu, Busan, Korea
yeonoh@tu.ac.kr

Abstract *- This paper studied robot systems and structures based on the adhesive force of magnets to develop wall-climbing robots using the magnetic force to enable climbing of a steel structure, such as ships, and exploration of their interior. The adhesive force was suggested in the form of a formula to select magnets required for the design of a wall-climbing robot utilizing magnetic force. The adhesive force based on the magnetic one should be reflected not only in the selection of the magnets but in the calculation of the torque required for the wheels. An analysis on the motor driving torque required depending on the location of the center of gravity(COG) to identify various relevant characteristics shows that a lower torque is required when COG is located closer to the center of the body of the robot and to the ground and that the same torque is produced at the front and rear wheels. Therefore, the finding that the location of COG should be closer to the ground and to the center of the body needs to be reflected in the design of wall-climbing robots. It also proposes a mechanism that guarantees smooth driving on a stiff slope and a comparison of any changes in the driving torque of the robot depending on the location of COG. In addition, changes witnessed in the body of the robot while moving were compared based on driving tests and simulation.*

Keywords — *driving torque, wall-climbing, mechanism, exploration robot, the center of gravity*

I. INTRODUCTION

Robots were developed to enhance operational efficiency and to make them do simple tasks instead of humans. Especially, the scope of their applications is further expanded to include robots designed to be employed in maritime or submarine areas, which are being studied. The main purpose of such robots used in this environment is to replace humans to explore the interior/exterior of ships. Especially, those employed for inspection are to secure safety, to prevent workers from safety-related accidents, and to enhance their operational efficiency.

Among exploration robots, there are wall-climbing ones, which climb the inclined plane of a large steel structure, targeted to be explored. The currently developed wall-climbing robots either run on wheels or are tracked or adopt the walking locomotion mode in some special cases [1~4]. An operating system of the continuous track is difficult to be used in a narrow and curved environment similar to the interior of ships due to the structure of the track. It is required to minimize the size of the platform of the climbing robots to overcome such a disadvantage, but difficulties in reducing the size due to the structure of the track pose a limitation in its application to the interior of ships [5].

This paper studied robot systems and structures based on the adhesive force of magnets to develop wall-climbing robots using the magnetic force to enable climbing of a steel structure, such as ships, and exploration of their interior. It also proposes a mechanism that guarantees smooth driving on a stiff slope and a comparison of any changes in driving torque of the robot depending on the location of the center of gravity (COG). In addition, changes witnessed in the body of the robot while moving were compared based on driving tests and simulations.

II. WALL CLIMBING ROBOT SYSTEM

Fig. 1 displays a conceptual diagram of the environment where the wall-climbing robots are used. The driving environment and system of such a robot reflected steel structures, such as ships, on which magnets can be attached. The user monitors and controls the robot in real-time at the control room, and the data is transmitted via a wired/wireless router. Command data required to control the robot is sent from the control room, which then receives a video signal. The command data sent from the control room is delivered to the controller on top of the targeted ship. The received signal is transferred to the robot via a signal wire connected to the cable roller. The robot is placed and attached on the surface of a steel structure, such as ships, and moves along the surface of the ship targeted upon the receipt of a signal sent from the control room. While it is moving, it receives real-time video footage of the surface of the ship from the attached camera and sends them via the controller to the control room.

This is an open access article under the CC BY-NC-ND license (http://creativecommons.org/licenses/by-nc-nd/4.0/)

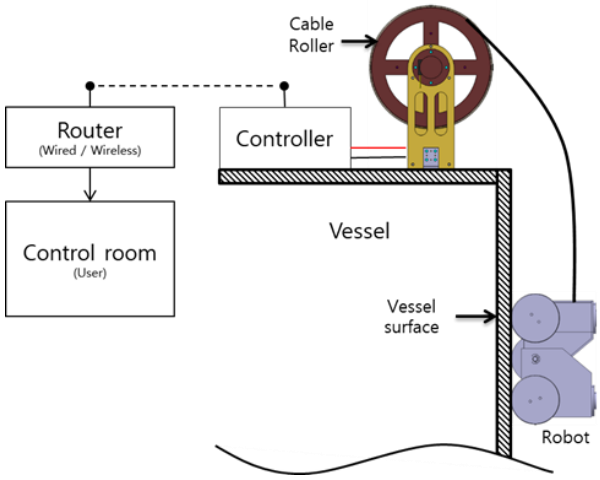

Fig.1 System Configuration

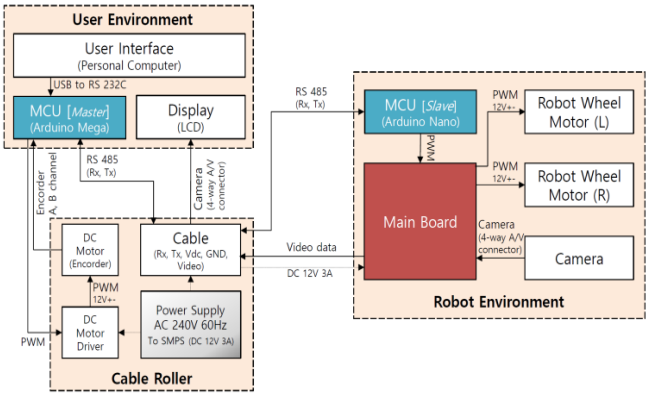

Fig. 2 System Block Diagram

As depicted in Fig. 2, the robot system consists mainly of the following three parts: user environment, control box, and robot environment. The user environment refers to an area where the ship operator observes the video clips from the camera attached to the robot in real-time and maneuvers its operation. For the user's easier access, GUI (Graphical User Interface) is provided to display videos filmed by the robot. GUI is composed as shown inFig. 3.

The second part, which is the control box, consists of devices required to control the robot.

The main control device is Arduino Mega MCU(Micro Controller Unit), which controls command data transmission and the cable roller. MCU receives a command via the wired/wireless router and sends the corresponding operation command to the robot. The command data from MCU for the operation of the robot is delivered via the signal wire. For this purpose, RS485 communication was adopted, which is usually used for long-distance communications as it is capable of data communication for up to 1.2 kilometers. The command delivered from the data is for the robot to move forward or backward, or rotate right or left, and when it moves forward (or downward), the wire is unwound from the cable roller, and when it moves backward (or upward), the wire is wound. At this moment, the robot receives and stores video data in real-time in the DVR (Digital Video Recorder) of the control box while on the move and simultaneously sends them in real-time via the monitor on the control box. The video data is utilized to maneuver the robot in the user environment.

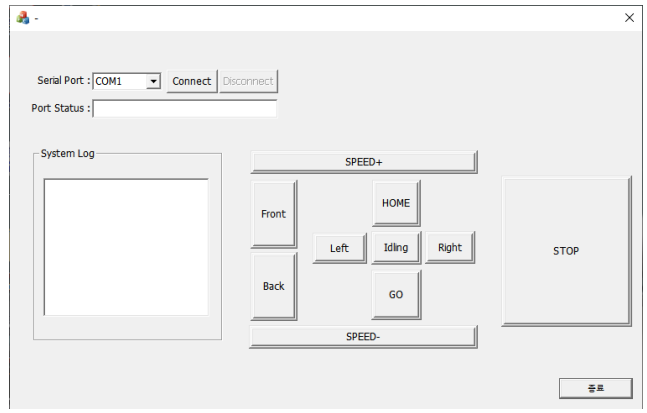

Fig. 3 Graphical User Interface

Lastly, the robot environment is made of a motor for the operation of the robot, a camera necessary for the transmission of videos, and the mainboard for power supply and control.

The mainboard is equipped with a 4ch motor driver, which enables the PWM control of the DC motor and a voltage output pin. The allowable voltage is up to 24V, and the communication protocol for motor control is processed based on hexadecimal commands.

III. DESIGN PARAMETER AND DRIVING TORQUE

A. Design Parameter

As a wall-climbing robot moves on the inclined plane, its center of gravity (COG) and location are crucial parameters. Therefore, it is important to find its COG. An interpretive approach was taken to calculate the COG of a complicatedly shaped object, such as assembled robots, by using a CAE program for a model assembled in 3D CAD. As a way to find COG, CATIA, a CAD/CAE program, was employed for its analysis. For the interpretation of COG, aluminum was chosen as the material of the frame of the robot, while steel was selected for the wheels and motor. The selection was made based on the parts used to produce the robot, and Table 1 lists the properties of each material. Fig. 4 and Fig. 5 display the interpretation results of COG of the wall-climbing robot. Table 2 shows its design parameters.

Table. 1 Material Property of Aluminum and Steel

Properties	Aluminum	Steel
Young Module (GPa)	70	200
Poisson ratio	0.346	0.266
Density (kg/m^3)	2710	7860
Thermal expansion (10^{-6}/K)	23.6	11.7
Yield Strength (MPa)	95	250

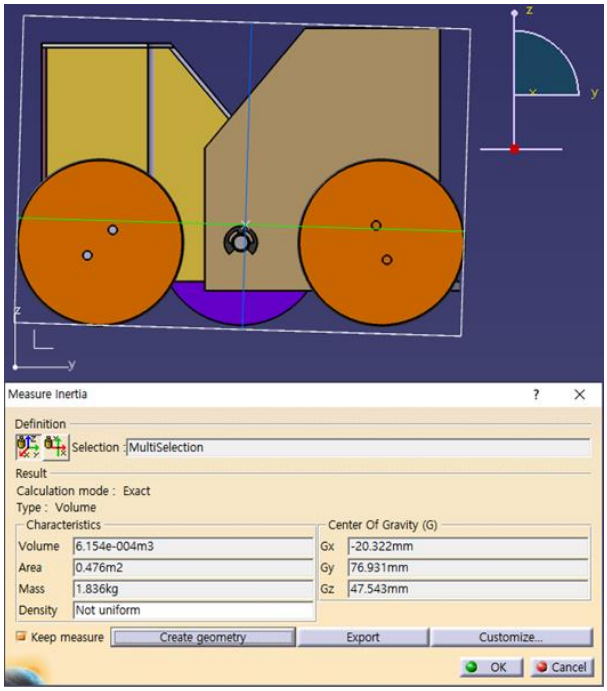

Fig 4. Center of Gravity in Wall Climbing Robot

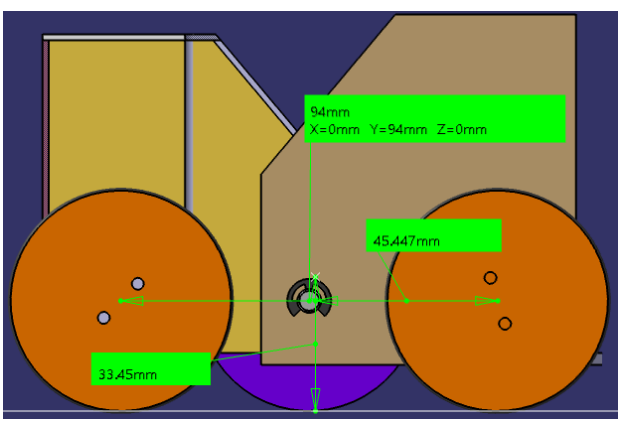

Fig. 5. Design Parameter from Center of Gravity

Table 2. Design Paarmeter of Wall Crimbing Robot

Parameters	K [m]	l [m]	h [m]	W [N]
Value	0.094	0.045447	0.03345	29.43

B. Calculation of Torque for Motor Selection

Motor torque is divided into the following two sections, as shown in Fig. 6: accelerating section and constant velocity section.

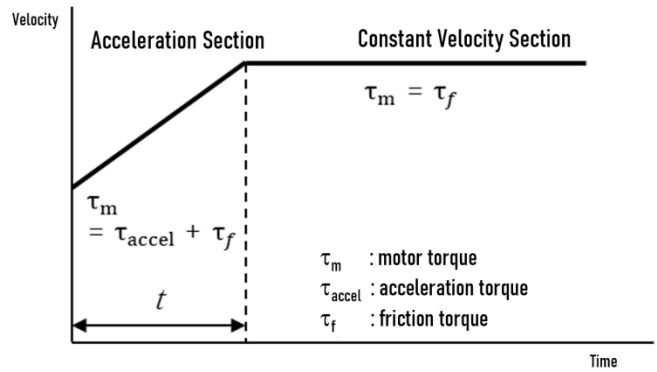

Fig. 6 Required Motor Torque

Motor torque (τ_m)required for the robot to move along a wall should reflect accelerating torque (τ_{accel}) and friction torque (τ_f) per time (t) taken to reach a certain velocity when the motor runs. In case it moves at a constant velocity, the required torque is the same as the friction one, but the torque required for the motor to accelerate is much larger than the one required for the constant velocity section as it is expressed in the sum of the accelerating and friction torques.

To this end, the accelerating torque is calculated first. It is expressed as follows [7]:

$$\tau_{\text{accel}} = \frac{J}{g} \times \frac{2\pi f}{t} \quad (1)$$

Jrefers to a moment of inertia based on the load of the wheels and is indicated as follows:

$$J = \frac{1}{2} W R^2 \quad (2)$$

The weight applied on the wheels expressed in equation(2) is the same as normal force (N_a, N_c)[8]. Therefore, the moment of inertia of the front (F) and rear (B) wheels are as follows:

$$J_F = \frac{1}{2} N_A R^2 \quad (3)$$

$$J_B = \frac{1}{2} N_C R^2 \quad (4)$$

Given these, the accelerating torque of the front and rear wheels using equation (1) can be expressed respectively as follows:

$$F_{\tau_{accel}} = \frac{J_F}{g} \times \frac{2\pi f}{t} \quad (5)$$

$$B_{\tau_{accel}} = \frac{J_B}{g} \times \frac{2\pi f}{t} \quad (6)$$

The friction torque of the front and rear wheels is expressed respectively in the following equation[7]:

$$F_{\tau_f} = \mu N_A R \quad (7)$$

$$B_{\tau_f} = \mu N_C R \qquad (8)$$

The bottom line is that the motor driving torque (τ_m)is calculated by summing up all of the accelerating and friction torques indicated inequation(5) to equation(8) and is expressed as follows:

$$F_{\tau_m} = F_{\tau_{accel}} F_{\tau_f} \qquad (9)$$

$$B_{\tau_m} = B_{\tau_{accel}} B_{\tau_f} \qquad (109)$$

The torque required to run the motor was calculated based on the above formulas, and the parameters reflected in the selection of a motor for this study are listed up in Table 3.

Table 3. Parameter of Motor Driving Torque

Parameters	Velocity	Acceleration Time(t)	Radius of Wheel (R)	Rotation Period (f)	Acceleration of Gravity (g)
Value	0.1m/s	0.5sec	0.0275m	0.579Rev./sec	$9.81\mathrm{m/s^2}$

The velocity of the mobile robot was set at 0.1m/s, while its acceleration time was 0.5sec. The period of rotation was defined as approx. 0.579rotations/sec, which can be calculated as approx. 34.7rpm.

Fig. 7 shows changes in the estimated motor driving torque of the front and rear wheels (F_{τ_m}, B_{τ_m}) when the coefficient of friction(μ) and the heading angle was made to range from 0.1 to 1 and from 0 to 180 degrees, respectively. Fig. 7(a) indicates the results without the safety factor being considered, whereas (B) reflected the safety factor of 1.5, reflecting the general safety factor.

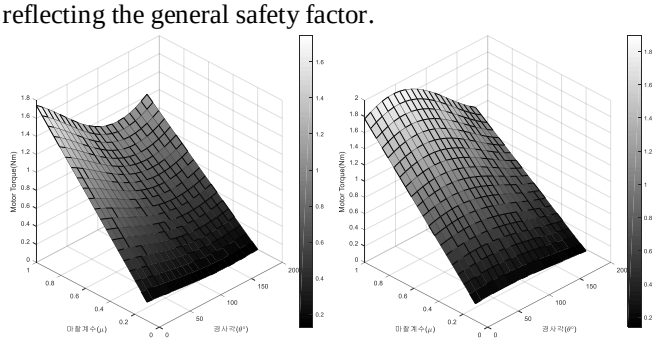

(a) Safety Factor Not Apply

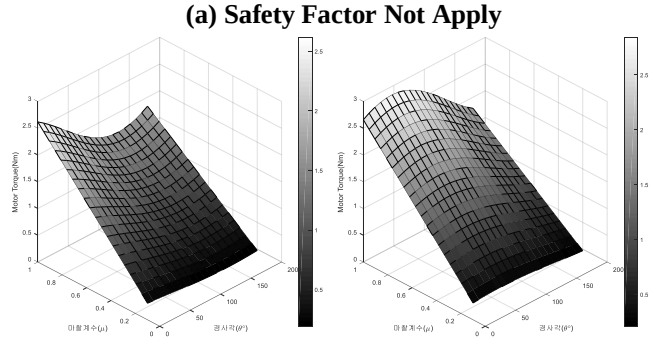

(b) Safety Factor: 1.5

Fig. 7 Result of Driving Torque (Left: Front, Right: Rare)

The graph in Fig. 7(b) indicates that the largest driving torque took place when the coefficient of friction of the rear wheels was 1 at the inclined angle of 60 degrees. Here, the motor driving torque was approx. 2.84Nm, which was temporarily required in the accelerating section. When the motor maintained a constant velocity, the torque diminished as the accelerating torque was excluded. Fig. 8 shows the motor driving torque required in the accelerating and constant velocity sections depending on the inclined angle of the slope when the coefficient of friction was 1.

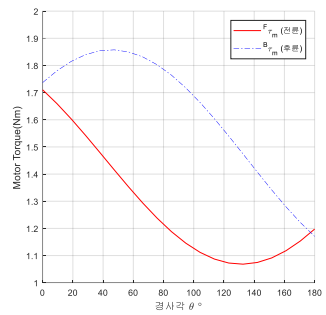

(a) Continuous Velocity

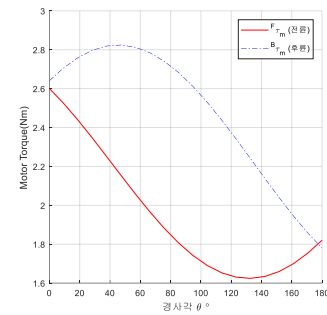

(b) Acceleration Velocity

Fig. 8Comparison between constant and acceleration-velocity torque

A look into the graphs in Fig. 8 suggests that the rear wheels show a larger driving torque than the front wheels, which can be attributed to the generation of a moment due to COG. To compare the effects of such a moment, changes were made to h, a parameter of the height from the ground to COG and to l, the distance between the center of rotation and COG, all of which are indicated in Fig. 9, and Fig. 10 show each change in the torque.

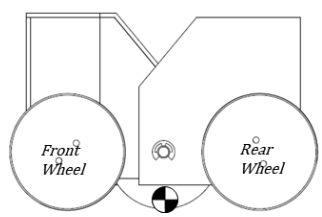

(a) h=0.001m, l=0.047m

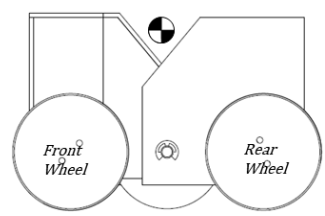

(b) h=0.1m, l=0.047m

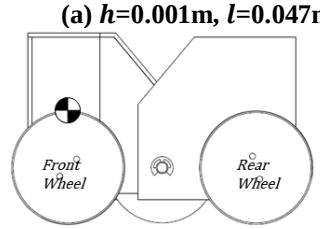

(c) h=0.05m, l=0.094m

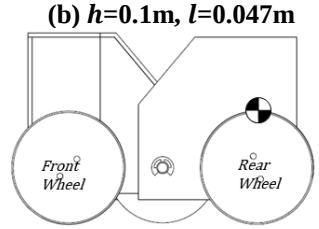

(d) h=0.05m, l=0.001m

Fig. 9 Changing Center of Gravity in Design Paramenter

Fig. 9 displays the four different locations of COG to find out about changes in the motor driving torque depending on the shifts in COG. To compare the torque, COG was placed in the upper, lower, right, or left parts of the body, given that the closer COG gets to the center of the body, the

larger a change of the moment becomes. (a) and (b) shows the cases where COG is placed on the lower or upper parts from the center of the robot, whereas (c) and (d) are for when COG is closer to each axle of the front and rear wheels. The calculations of the motor driving torque required depending on the location of CGO are indicated in Fig. 10.

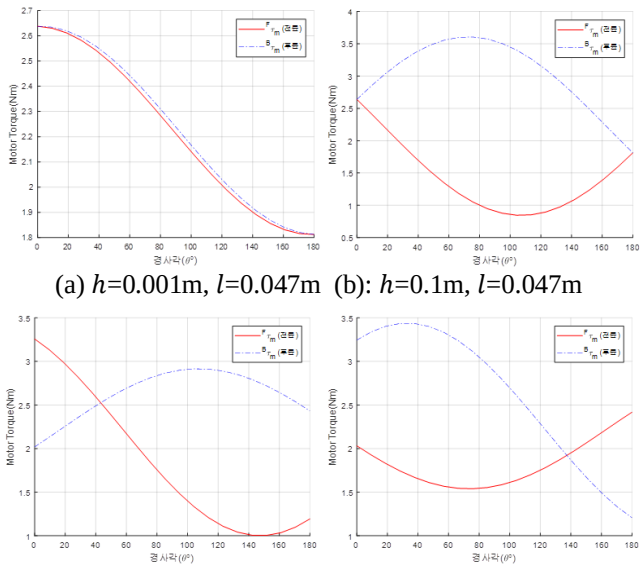

(a) h=0.001m, l=0.047m (b): h=0.1m, l=0.047m

(c) h=0.05m, l=0.094m (d) h=0.05m, l=0.001m

Fig. 10 Result of Driving Torque by Changing Center of Gravity

Fig 10demonstrates that all parameters except for h and$l$ are the same for all of the four cases that show different torque values depending on the location of COG, with the safety factor of 1.5 being applied. When the graphs are categorized per type of COG, (a), and (b) exhibit the changes only in h, and (c) and (d) are for changes in$l$. First of all, for the graphs reflecting only the changes in l, (c) has COG in the front wheels, whereas (d) has it located in the rear ones. Furthermore, the motor driving torque of the front and rear wheels presented in (c) and (d) graphs move in an opposite direction at the inclined angle of 40° and 140°, respectively. This is attributed to the effect of a moment caused by changes in the inclined angle, which acts in the opposite direction, as shown in Fig. 11.

Therefore, it is found that as for changes in COG and inclined angle, the vertical distance from the center of rotation (C) to the weight (w) switches its direction from -X to +X or from +Xto–X at a certain inclined angle, signaling that the moment acts in the opposite direction.

As for changes only in l, (c) and (d) of Fig. 10 show symmetry of the wheels, and their motor driving torque was found to be similar. However, the results demonstrated in (a) and (b), which are related to changes only in h, are remarkably different from one another. COG in (a) is placed in the center of the robot, very close to the ground, and the graph shows that the motor driving torque required at the front and rear wheels are very similar. In the case of (b), however, where COG is located in the upper part of the robot, the motor driving torque changes significantly depending on the inclined angle. In addition, (a) and (b) indicate that the torque at the front and rear wheels are the same at the inclined angle of 0° and 180°.

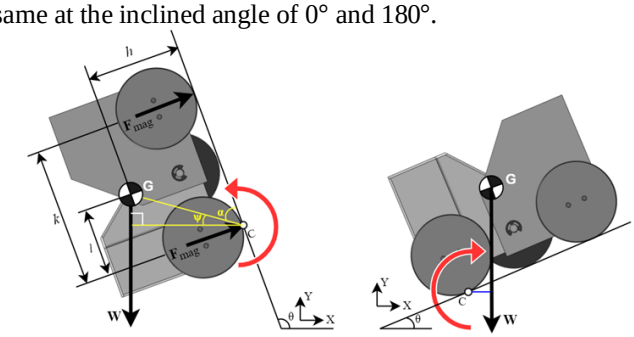

Fig. 11 Moment Chang due to Climbing Angle at Joint axis

An analysis on the motor driving torque required depending on the location of COG to identify various characteristics shows that a lower torque is required when COG is located closer to the center of the body of the robot and to the ground and that the same torque is produced at the front and rear wheels. Therefore, the finding that the location of COG should be closer to the ground and to the center of the body needs to be reflected in the design of wall-climbing robots.

IV. CONCLUSIONS

A mechanism that guarantees stable driving of the robot in the face of a sharp change on the inclined plane was proposed. This enables a mobile robot to flexibly respond to a sudden change in the inclined angle as it moves to mount to the slope thanks to the joints placed on the center of the body.

The adhesive force was suggested in the form of a formula to select magnets required for the design of a wall-climbing robot utilizing magnetic force. The adhesive force based on the magnetic one should be reflected not only in the selection of the magnets but in the calculation of the torque required for the wheels.

An analysis on the motor driving torque required depending on the location of COG to identify various relevant characteristics shows that a lower torque is required when COG is located closer to the center of the body of the robot and to the ground and that the same torque is produced at the front and rear wheels. Therefore, the finding that the location of COG should be closer to the ground and to the center of the body needs to be reflected in the design of wall-climbing robots.

REFERENCES

[1] S. D. Kwon, S. J. Kim, S. Y. Kim, S. H. Kim, Design of wall-climbing mobile platform by modeling of attachable and traction force, in Proc. The 2010 Fall Conference of The Korean Association of Immunologists, Korean Society Of Precision Engineering, (2010) 239-240.

[2] H. R. Choi, J. H. Lee, Development of wall-climbing robot, in Proc. 1999 Spring Conference of The Korean Association of Immunologists, Korean Society Of Precision Engineering, (1999) 3-6.

[3] H. Kim, K. Seo, J. Kim, H. Kim, Design of tracked wheel mechanism for wall climbing robot, in Proc. 2010 Fall Conference of The Korean Association of Immunologists, Korean Society Of Precision Engineering, (2010) 215-216.

[4] S. H. Park, K. J. Seo, J. R. Choi, D. H. Kwon, J. H. Bang, S. G. Kim, Development of the wall-climbing robot using New Mechanism, in Proc. 2016 Fall Conference of the Korean Association of Immunologists, Korean Society of Precision Engineering, (2016) 150-151.

[5] S. C. Han, J. Y. Lee, J. H. Kim, Design of hybrid magnet wheels using 3d finite element analysis for the wall-climbing robot, Journal of the Society of Naval Architects of Korea, 47(1) (2010) 88-89.

[6] R.C. Hibbeler, Kai Beng Yap, Mechanics for Engineers: DYNAMICS 13th Edition, (2015)

[7] Jae Young Joo, Jae Young Joo, Yeon Taek OH, Study of a wall-climbing robot having proposition of stable mechanism on inclined plne based on magnetic force, Journal of Automation and control engineering, 7(1) (2019) 36~40.

[8] H. Yi, E. Kim, S. Han, Guideline for the design of wall-climbing mobile robot using permanent magnetic wheels, in Proc. 2002 Fall Conference of The Korean Association of Immunologists, Korean Society Of Precision Engineering, (2002) 548-553.

[9] Yeon Taek OH, Study of a wall-climbing robot having magnetic force, J. Korean Soc. Mech. Technol, 22(6) (2020) 1001~1005.

[10] Nicholson, J. W., and Healey, A. J., The Present State of Autonomous Underwater Vehicle (AUV) Application and Technologies, Marine Technology Society Journal, 42(1) (2008) 44-52.

[11] Ura, T., Tabuchi, H., Obara, T., Maeda, H., and Yamato, H., Development of Autonomous Vehicle with a Closed Cycle Diesel Engine, Proc. 18th Joint Meeting UJNR Marine Facilities Panel, (1993) 170-188.

[12] Bradley, A. M., Feezor, M. D., Singh, H., and Sorrell, F. Y., Power System for Autonomous Underwater Vehicle, IEEE Journal of Oceanic Engineering, 26(4) (2001) 526-538.

[13] Sibenac, M., Podder, T., Kirkwood, W., and Thomas, H., Autonomous Underwater Vehicles for Ocean Research: Current Needs and State of the Art Technologies, Marine Technology Society Journal, 38(2) (2004) 63-72.

[14] Stokey, R. A. et al., Development of REMUS 600 Autonomous Underwater Vehicle, Proc. MTS/IEEE Oceans, (2005).

[15] McEwen, R. H., Thomas, D., Weber, D., and Psota, F., Performance of an AUV Navigation System at Arctic Latitudes," IEEE Journal of Oceanic Engineering, 30(2) (2005) 443-454.

[16] Miline, D. H., Underwater Acoustic Positioning Systems, Gulf Publishing, Houston, (1983).

[17] Kinsey, J. C., Eustice, R. M., and Whitcomb, L. L., Underwater Vehicle Navigation: Recent Advances and New Challenges, Proc. IFAC Conf. on Maneuvering and Control of Marine Craft, Lisbon, Portugal, (2006).

[18] Ribas, D., Ridao, P., Tardos, J. D., and Neira, J., Underwater SLAM in Man-Made Structured Environments, Journal of Field Robotics, DOI 10. 1002, (2008) 1-24.

[19] Fairfield, N., Kantor, G. and Wettergree, D., Real-time SLAM with Octree Evidence Grids for Exploration in Underwater Tunnels, Journal of Field Robotics, 24 (2007) 3-21.

[20] Y. T. OH, Evaluation of joint driving torque and finite element analysis in articulate robot through the simulation of multi-body dynamics, International Jpournal of Innovative Technology and Exploring Engineeing, 8(11) (2019) 682-686.

[21] Ig Mo Koo1, Young Kouk Song,Hyungpil Moon, Sun Kyu Park, HyoukRyeol Choi, Design and Control of Wall Climbing Robot Using Impeller, Journal of Korea Robotics Society, 5(3) (2010) 177-185.

[22] X. Daijun, G. Xueshan, W. Xiaobing, F. Ningjun, L. Kejie, K. Koki, Suction Ability Analyses of a Novel Wall Climbing Robot, Proceedings of IEEE International Conference on Robotics and Biomimetics, (2006) 1506-1511.

[23] Y. K. Song, C. M. Lee, I. M. Koo, D. T. Trong , H. Moon, H. R. Choi, Development of Wall Climbing Robotic System for Inspection Purpose, in Proc. IEEE/RSJ Int. Conf. Intelligent Robots and Systems, (2008) 1990-1995.